Coal derived rates of atmospheric dust deposition during the Permian.

Chris Marshall, David J. Large

University of Nottingham, University Park, Nottingham, NG7 2RD

Nicholas G. Heavens

Hampton University, Hampton, VA, 23669, USA

Corresponding author: david.large@nottingham.ac.uk

Abstract.

Despite widespread evidence for atmospheric dust deposition prior to the Quaternary, quantitative rate data remains sparse. As dust influences both climate and biological productivity, the absence of quantitative dust data limits the comprehensiveness of models of pre-Quaternary climate and biogeochemical cycles. Here, we propose that inorganic matter contained in coal primarily records atmospheric dust deposition. To test this, we use the average concentration of inorganic matter in Permian coal to map global patterns and deposition rates of atmospheric dust over Pangea. The dust accumulation rate is calculated assuming Permian peat carbon accumulation rates in temperate climates were similar to Holocene rates and accounting for the loss of carbon during coalification. Coal-derived rates vary from 0.02 to 25 g m^{-2} yr^{-1}, values that fall within the present-day global range. A well constrained East-West pattern of dust deposition corresponding to expected palaeoclimate gradients extends across Gondwana with maximum dust deposition rates occurring close to arid regions. A similar pattern is partially defined over the northern hemisphere. Patterns are consistent with the presence of two large global dust plumes centred on the tropics. The spatial patterns of dust deposition also were compared to dust cycle simulations for the Permian made

with the Community Climate System Model version 3 (CCSM3). Key differences between the simulations and the coal data are the lack of evidence for an Antarctic dust source, higher than expected dust deposition over N and S China and greater dust deposition rates over Western Gondwana. This new coal-based dust accumulation rate data expands the pre-Neogene quantitative record of atmospheric dust and can help to inform and validate models of global circulation and biogeochemical cycles over the past 350 Myr.

Keywords: Permian, Pangea, dust, coal, atmospheric deposition

1. Introduction.

Mineral dust influences globally important terrestrial and marine biogeochemical processes, particularly the carbon cycle, by seeding oceanic and terrestrial ecosystems with phytonutrients such as iron and phosphorus (Boyd and Ellwood, 2010; Bristow et al., 2010; Evan et al., 2011; Okin et al., 2011). Mineral dust also influences climate via its influence on albedo and cloud nucleation (Prenni et al., 2009; Sugden et al., 2009). Quaternary dust deposition records are predominantly obtained from ice-cores (Lambert et al., 2008), deep marine sediments (McGee et al., 2013), and peat (Le Roux et al., 2012). Of these only peat is extensively preserved in the pre-Quaternary geological record, where it occurs as coal and lignite in a wide range of palaeogeographic settings.

Records of atmospheric dust deposition prior to the Quaternary are abundant but mostly have gone unrecognized (Gabbott et al., 2010; Retallack, 2011; Retallack et al 2003: Retallack et al 2012; Soreghan et al., 2008a) and do not readily yield quantifiable rates of dust deposition. In terrestrial settings, there are multiple examples of alternating loess and palaeosol accumulation analogous to deposits in the Chinese Loess Plateau (Soreghan et al.,

2008a; Soreghan et al., 2008b; Soreghan et al., 2014). In shallow marine settings, a distinctive facies of fine dust is often observed at lowstands (Soreghan et al., 2008b; Sur et al., 2010). In one case, the concentration of silicate minerals in a shallow marine carbonate deposit was used to estimate dust accumulation rates (DAR) that ranged over the course of a presumptive glacial–interglacial cycle from 0.07 to 160 g m^{-2} yr^{-1} (note that the maximum is uncertain by an order of magnitude) (Sur et al., 2010). Similar data also exists for two other sites (Patterson, 2011; Stagner, 2008). In principle, DAR could also be estimated from loess–palaeosol deposits under an assumption of layers correlating to orbital cycles (Soreghan et al., 2014).

At present, however, all of this data is confined to the palaeotropics, spans Late Carboniferous to Early Permian time, and is two orders of magnitude less abundant than DAR data at the Last Glacial Maximum (Maher et al., 2010). Consequently, if coal and lignite, like peat, could be used to estimate DAR, the extant quantitative record of dust prior to the Quaternary could be greatly expanded. This greater volume of data would allow dust to be considered in models of global processes for times as early as 350 Ma, when the first coals were deposited.

Using carbon accumulation rates from Holocene peat in conjunction with realistic rates of dust deposition, Large and Marshall (2014) showed that the titanium concentration in Cenozoic coal and lignite, and therefore a high proportion of the inorganic matter in coal, can be accounted for by atmospheric dust deposition into the precursor peat. Conversely, we propose that given coal composition data of sufficient geographic extent and a reasonable estimate of the carbon accumulation rate in the precursor peat, it should be possible to constrain mineral dust deposition rates and map global patterns of dust deposition.

The Permian is an ideal period to test this proposal. During the Permian, globally extensive mid to high-latitude peat deposits accumulated across the supercontinent Pangea and the continental configuration was relatively stable (Langford et al., 1992). Over the course of the Early Permian, the subtropical arid belts expanded to meet at the Equator (Boucot et al., 2013). From that point, the zones of aridity were relatively stable (Scotese, 2001). Widespread loess deposits near the Equator in the Early Permian and Middle Permian (Soreghan et al., 2008a) as well as other indicators of widespread tropical and subtropical aridity (Boucot et al., 2013) strongly suggest that Permian peat deposits must have been exposed to dust transported from arid dust source regions that spanned the low latitudes. Particularly useful from this perspective is the laterally contiguous Gondwana coal belt that extended from Brazil to Australia (Langford et al., 1992).

Regional differences in Gondwana coal, notably high concentrations of dispersed inorganic matter (ash) in coal from Brazil, South Africa and India are attributed to locally variable deposition processes (Glasspool, 2003; Jha et al., 2014; Silva and Kalkreuth, 2005). This has resulted in multiple local coal deposition models, none of which consider that regional variations in the concentration of inorganic matter in the coal may have been primarily determined by patterns of global atmospheric dust deposition. Also, an incomplete understanding of the large scale controls on coal ash content is likely to have profound consequences for coal exploration and mine development, where ash concentration is an important determinant of coal quality.

Our approach is to collate data on the average concentration of inorganic matter in Permian coal and determine whether this data displays a global pattern consistent with qualitative and quantitative climate modelling. Locally independent syn- and post-depositional processes cannot explain a global pattern, and we postulate that the only plausible explanation for such a pattern is global atmospheric dust transport and deposition.

Coal derived dust accumulation rates are then compared to the results of quantitative simulations of Permian dust deposition in greenhouse and icehouse conditions as well as the limited dust accumulation rate data available from other sources and the implications discussed.

2. Methods.

2.1 Basis for determining DAR from coal.

This approach assumes that the major lithophile elements (Si, Al, Mg, Fe, Ca, Mn, K, Na, Ti) that constitute the bulk of the inorganic constituents in coal (Bragg et al, 1998; Tewalt et al, 2010) originate predominantly from silicates and oxides in atmospheric dust. This assumption refers to the origin of the elements not to the association of these elements in the coal with mineral matter, organic matter etc. which can be highly variable (Ward, 2002). Other sources of inorganic elements in coal are shallow and deep groundwater (syn- and post-deposition) and water borne clastic sediment, both of which are controlled by local not global processes and should therefore not display global trends. Furthermore, water borne clastic deposition rates in coal forming environments (floodplains, estuaries and deltas) are typically in the range 0.02 to 1 mm per year (Einsele, 2000) which at typical bulk soil densities of 1200 to 1600 g/cm^3 corresponds to mass deposition rates of 24 to 1600 g/m^2/yr. Given a realistic estimate of time and carbon balance (Large and Marshall, 2014) the supply of clastic matter to peat at all but the lowest of these rates (<35 g/m^2/yr) could not result in the production of coal, and even the lowest of these rates would produce a poor quality coal.

The measure we use for these elements is the reported ash concentration generated by high temperature ashing (Vassilev and Tascon, 2003) a process that converts the elements back to oxides. Some more volatile elements are lost during high temperature ashing (Vassilev and Tascon, 2003) but the major lithophile elements are preserved.

Many elements present in mineral dust, which has an average composition (Lawrence and Neff, 2009) similar to upper continental crust, are potentially soluble in wet, acidic peat-forming environments so ideally a highly insoluble lithophile element such as titanium should be used as a measure of dust deposition. However, only 280 samples were found with reported titanium concentrations. This reduction in sample size would severely limit the extent and resolution of the data, so we have used the ash concentration in the coal rather than titanium. In support of this approach, atmospheric dust has been shown to be relatively stable in peat (Zaccone et al., 2013) and ash concentration correlates positively with the concentration of titanium (Fig. 1); evidence that the ash is dominated by lithophile elements introduced into the peat during deposition.

A major uncertainty is the assumption that Holocene carbon accumulation rates are applicable in the Permian. The basis for this assumption is that carbon accumulation rates are primarily determined by the balance between productivity and decay in the precursor peat which in turn is determined by climate (Clymo et al., 1998). Given that Permian palaeoclimate and soil productivity in Gondwana appear to have been similar to that found in the peat bearing boreal and temperate regions of the Northern Hemisphere today (Gibbs et al., 2002; Retallack, 1999) and that the C3 photosynthetic pathway dominated both systems (Beerling and Woodward, 2001) this seems a reasonable assumption. More importantly this assumption is clear and the approach used is easily adapted by applying different quantitative models of the link between carbon accumulation rate, flora and climate to the collated data. As bounds to the uncertainty, we consider the consequence of halving or doubling the peat carbon accumulation rate.

2.2 Calculation of coal derived DAR.

In a particular coal the rate of mineral dust deposition is calculated using the ash concentration, the palaeolatitude and the concentration of carbon on a dry ash free basis. Palaeo-latitude determined using PaleoGIS is used in conjunction with a linear model of the latitudinal variation in peat carbon accumulation rate (Large and Marshall, 2014) to estimate the long-term carbon accumulation rate in the precursor Permian peat. The proportion of carbon lost during the transformation of peat to coal is determined by modelling the relationship between the mass of carbon lost and the dry ash-free carbon concentration of the coal (Large and Marshall, 2014). In combination the measure of carbon input and carbon loss enable the time required to accumulate a given mass of carbon and associated ash to be calculated and hence calculation of the mineral dust accumulation rate required to account for the inorganic matter in the coal.

Carbon accumulation rate in the precursor Permian peat is calculated using a linear regression to a graph of Holocene peat carbon accumulation rate versus latitude (Large and Marshall, 2014). The proportion of the carbon lost during coalification is determined relative to a woody peat starting composition which on a dry ash free basis contains 58.6% carbon, 5.4% hydrogen and 34.7% oxygen (Large and Marshall, 2014). The proportion of carbon remaining is then determined assuming that during coalification all carbon is lost as methane and carbon dioxide. The trend of carbon loss was empirically fitted to the observed trend in coal composition with increasing rank plotted on a van Krevelen diagram of O/C vs. H/C (Large and Marshall, 2014). The proportion of carbon retained in the coal relative to the original peat is then expressed via the fourth order polynomial fit to a graph of carbon concentration in the coal on a dry ash free basis vs. the proportion of carbon retained relative to that in the precursor peat.

$$p= 33.332c^4 - 117.25c^3+155.18c^2-92.699c+21.733$$

p = proportion of C remaining relative to that in precursor peat

c = concentration of carbon in the coal on a dry ash free basis

2.3 Generation of Permian Coal Database

A coal geodatabase (Supplementary Table 1, Table 2 and Supplementary Database References) containing ash concentration, current latitude and longitude and the estimated deposition rates of mineral dust, iron and phosphorus from 759 Permian coals from across Pangea was created in ESRI ArcGIS 10.1 and transformed using the UTIG Kungurian epoch (272-283 Myr) plate model in PaleoGIS to provide a palaeolatitude and palaeolongitude position for each data point. A mid-Permian Kungurian palaeogeography was chosen as at this time Gondwana peatland was at its most contiguous (Langford et al., 1992). Stratigraphically, Brazilian and South African coals were deposited during the Artinskian-Kungurian, Indian coals during the Artinskian-Kungurian and Capitanian-Wuchiapingian with Australian coals encompassing the entire Permian (Langford et al., 1992; Fig. 2). In the Northern hemisphere, US coals and N. China coals were deposited in the Asselian-Artinskian and South China coals represent Wuchiapingian-Changhsingian deposition (Fig.2). Extensive Russian Permian coal deposits (some as thick as 20m) are under-represented within the dataset primarily due to lack of exploitation leading to very little published coal quality data (Thomas, 2013). In selecting data multiple values from a single location were averaged and values that encompassed known sediment partings within the coal were excluded. Where coal carbon concentration data was missing an average value for coal from the same region was used.

2.4 Data Contouring

The contouring method applied is the standard ordinary kriging method in the ArcGIS Geostatistical Analyst Toolbox. Prior to analysis the data was checked for normality and the presence of global trends. Second order trend removal was applied to account for a strong E-W trend and a lesser N-S trend. This second order trend observed is the trend expected from patterns of global dust transport. Once detrended, ordinary kriging was then applied to the residuals and the prediction surface contour maps created. Post kriging the model was optimised by accounting for anisotropy in the existing spherical semivariogram. The resulting prediction map was cross-validated to examine whether the model was reasonable for contour map production and a standard error map was produced (Fig. 3). Greatest errors are seen within low sample density regions; reflecting the sporadic nature of the geological record (Fig. 3). Interpolations were clipped to data points in order to limit displayed results to areas with sufficient data coverage and the least uncertainty. Variable uncertainty within the contoured area is illustrated on contoured plots of standard error (Fig. 3).

2.5 Dust deposition modelling

To simulate dust deposition during the Permian, multiple simulations were performed with the Community Climate System Model version 3 (CCSM3) at a T31 resolution (3.75°); configured for an Asselian–Sakmarian palaeogeography; and under a diversity of greenhouse gas levels, sea level, and glacial extent. These simulations were run to approximate energetic balance between the ocean and atmosphere under a uniform aerosol forcing. These simulations and the range of climates within them are fully described by Heavens et al. (Heavens et al., 2015). This study focuses on two of these simulations: greenhouse.noglaciation (a simulation corresponding to a warm greenhouse interval with pCO_2 = 2500 ppmv and no land ice) and icehouse.glaciation.polar (a simulation corresponding to an icehouse interval with pCO_2 = 250 ppmv, a large ice sheet near the South Pole, and a small ice sheet in northern Angara).

Using these simulations as an initial condition, the emission, transport, and deposition of radiatively passive dust (0.1—10 μm in size) was simulated using a modified version of the model routines used by Mahowald et al. (2006b) and Yoshioka et al. (2007). These combine the Dust Entrainment and Deposition (DEAD) model (Zender et al., 2003a) and the Model of Atmospheric Transport and Chemistry (MATCH) (Luo et al., 2003).

Following the observations of Okin (2008) that dust emission can come from more vegetated regions than previously believed the dust emission routines of Mahowald et al. (2006b) were modified by increasing the vegetation area index (VAI) threshold for emission from 0.1 m^2 m^{-2} to 0.3 m^2 m^{-2}. Second, the size distribution of the emitted dust was modified to agree with the observationally validated physical model of Kok (2011): 0.1—1.0 μm 1.1%; 1.0—2.5 μm 8.7%; 2.5—5.0 μm 27.7%; and 5.0—10.0 μm 62.5%. Mahowald et al. (2006a) made the following assignment of the emitted flux to bins: 0.1—1.0 μm 3.8%; 1.0—2.5 μm 11%; 2.5—5.0 μm 17%; and 5.0—10.0 μm 67%.

The model routines also were modified to better represent interactions between climate, vegetation, and dust emission. The simulations reported by Heavens et al. (2015) only use two vegetation maps to account for the effect of vegetation on moisture transport, albedo, and aerodynamic roughness. While the model climate is weakly sensitive to the choice of vegetation map (Heavens et al., 2015), dust emission in the model is strongly sensitive to vegetation cover. Therefore, not accounting for changes in vegetation due to climate would mute the simulated dust cycle's sensitivity to climate. At the same time, fully changing the vegetation map would slightly change the climate. Therefore, the simulations were modified so that the vegetation cover thresholds for dust emission would be based on the biomes predicted by the equilibrium vegetation model BIOME4 (Kaplan et al., 2003) when forced by the model climate. However, the vegetation input to the model that was relevant to moisture transport, albedo, and aerodynamic roughness was left unchanged.

The dust emission formulations in the model predict dust emission under the assumption that dust-containing sediment is always available across the entirety of the grid cell. In fact, such sediment is heterogeneously distributed on the Earth (Ginoux et al., 2001). Therefore, dust cycle simulations typically multiply the predicted dust emission by a geographically varying soil erodibility factor (sometimes called a source function, *S*) (Ginoux et al., 2001; Mahowald et al., 2006b). This factor can be estimated on theoretical grounds (Zender et al., 2003b) or by tuning the model to match observations (Mahowald et al., 2006b). However, this factor cannot be estimated for the Permian on theoretical grounds without higher resolution palaeotopographic information than available. Moreover, there is insufficient observational information other than the coal-derived data to tune a model. Therefore, *S* was set to 0.0651, the average value on land for the Earth's current geography according to the geomorphic hypothesis (Zender et al., 2003b).

For purposes of comparison with the coal derived data, the output of the model was shifted 30 degrees west to better align the palaeogeography used for compiling the data. The dust deposition and dust emission data were scaled so that dust deposition in the palaeogeographic location of western Brazil (24° S, 117.5° W in the shifted reference frame) is 32 g m^{-2} yr^{-1}. This adjustment increases global dust deposition and emission by 81 % in the greenhouse interval simulation and by 7.6% in the icehouse interval simulation.

3. Results and Discussion

Ash concentration in the coal (Fig. 4A) displays a systematic longitudinal decrease from West to East across Gondwana. Highest average ash concentrations (30-45%) occur in South America, intermediate concentrations in Southern Africa (20-30%) and India (10-30%) and the lowest concentrations in Australia and Antarctica (<15%). In western Gondwana ash concentrations also increase northwards. Variable, locally controlled deposition processes

cannot explain the presence of this systematic global pattern. In the northern hemisphere ash concentrations are low at higher latitude (<10%), higher in the tropics (10-30%) and highest (30-40%) in low latitude coal from the western continental interior.

Coal-derived DAR (Fig 4B) reach 25 g m^{-2} yr^{-1} close to western Pangea and decrease systematically away from these regions. The assumed latitudinal gradient in peat carbon accumulation rate produces strong latitudinal gradients in the rate of dust deposition over Gondwana. In size, shape and extent the magnitude and pattern of dust deposition over Gondwana is similar to what would be expected from a large dust plume centred on the Tropic of Capricorn.

Simulated dust emission during greenhouse.noglaciation conditions (Fig. 5A) predicts dust source regions concentrated in equatorial western Pangea, with a distinct secondary source region located within central-west Antarctica. The icehouse.glaciation.polar emission simulation (Fig. 5B) also predicts major dust source regions in equatorial western Pangea with secondary dust source regions along south-west Pangea and in Angara. Unlike the greenhouse.noglaciation simulation it does not predict an Antarctic source region which is primarily attributed to ice cover.

Simulated DAR in both the greenhouse.noglaciation (Fig 6A) and the icehouse.glaciation.polar simulations (Fig. 6B) are highest in western Pangea decreasing westward as expected from the westward transport of dust from areas of dust emission. In the greenhouse.noglaciation simulation the extent of the Gondwana and Euramerica dust plume is more limited than during icehouse conditions likely due to the effects of increased vegetation and therefore decreased erodability. In this simulation relatively low DAR are predicted in North China, whereas in the icehouse.glaciation.polar simulation the Angaran dust source is much stronger augmenting dust transport eastward. Another difference

between the two simulations is the lack of an Antarctic dust plume in the icehouse.glaciation.polar simulation reflecting glaciation in this area at this time.

Comparison between the coal derived DAR data and simulated DAR data is inherently uncertain due to the indefinite nature of Permian source characteristics used in the simulations (as detailed in the methodology). However, the source characteristics are based on reasoned assumptions derived from the best currently available data. Comparison, however tentative, is made on this basis and can be revised in light of better or different source characteristics. Another important caveat is that the coal data can only represent regions and periods during which peat could accumulate and therefore does not represent drier or dustier conditions during which peat accumulation would be impossible. Over a certain DAR threshold of about 35 g m^{-2} yr^{-2} virtually any coal formed would be uneconomic (> 50% ash), probably under-reported and peat would be replaced by loess type deposits.

Coal-derived DAR (Fig 4B) and both the simulated DAR (Fig. 6) produce broadly similar dust deposition rates (0.01 – 30 g m^{-2} a^{-1}) which fall within the Neogene/Modern range. Simulated DAR exceeds this range in the centre of arid regions, where very high dust deposition rates and aridity preclude coal formation.

The greenhouse.noglaciation simulation and coal-derived DAR are similar in western Pangea with the exception that the coal-derived data shows extension of the equatorial Gondwana dust plume further south than simulated. This may indicate that dust source regions extended down the western edge of Gondwana, a pattern that is present within the icehouse.glaciation.polar simulation. This may be attributed to the presence of a colder coastal current during the earlier part of the mid Permian when western coals were still forming under conditions of low CO_2. In support of this, earlier and more arid Permian deposits that dominate data from the USA and Brazil, have lower Ti concentrations in the

coal ash. These lower Ti concentrations are closer to values expected in mean upper continental crust and consistent with lower intensity chemical weathering in the early Permian (Yang et al., 2014).

A key difference between the simulation and coal-derived DAR data is the lack of evidence for a significant Antarctic dust source in coal-derived DAR data. This may be due to a number of reasons including that the Antarctic region was glaciated, less arid than the simulation suggests or that the latitudinal gradient used in carbon accumulation is incorrect. The latter suggestion is considered unlikely as even when doubled the coal-derived DAR rates remain well below those predicted by the simulation. The best fit for the coal-derived DAR data is produced within the icehouse.glaciation.polar simulation (Fig. 6B). In this simulation the Antarctic dust source is very small, indicating that the period of eastern Gondwanan coal formation may represent a cooler period that favoured water storage in peatland and the associated accumulation of carbon and that Antarctica was glaciated and/or blanketed by extensive vegetation that suppressed dust emission.

Another discrepancy between the greenhouse.noglaciation simulation (Fig. 6A) and coal-derived DAR maps/icehouse.glaciation.polar simulation (Fig. 4B; 6B) is the extent to which the Angaran Shield is a dust source. Coal-derived DAR and the simulated icehouse.glaciation.polar DAR maps indicate that North China and most particularly the later South China coals experienced consistently elevated dust deposition during their formation. In the case of North China this may reflect strengthening and extension of the Angaran shield dust plume, possibly reflecting a propensity of the region to be eroded and generate silt sized particles. In support of this, the Ti concentrations in these coals are undifferentiated from most Pangean coal (Fig.1) indicating a similar general crustal dust source. In contrast to North China, ash in coal from South China is more Ti-enriched (Fig.1). This may be due to the known volcanic influence (Dai et al., 2012) and formation at low latitude both of which

should result in more weathered Ti-enriched dust source regions and depositional environments (Yang et al., 2014). A volcanic influence might also explain what appear to be two distinct trends within the South China data (Fig.1), one Ti enriched and the other aligned with global trend observed in Permian coal data from the other regions. Inorganic coal data from Brazil also occurs in two distinct clusters (Fig.1.), one that aligns with the global trend and another that may indicate the influence of a titanium depleted ash. The titanium depleted ash could represent less weathered material closer in composition to average upper continental crust (Li, 2000) which could be dust sourced under colder conditions or may represent a fluvial clastic influence.

While the simulated DAR magnitude was scaled to match coal DAR in west Brazil (see Methods), this adjustment was small enough to suggest that the simulated magnitude of DAR is within a factor of 2 of the coal DAR. Therefore, coal-derived dust deposition rates match the expected deposition rates for a planet with the average soil erodibility factor of the present day, that is, covered with dust in the same proportion as today. This result suggests that surface dust availability was not radically different in the Permian than today. However, theoretical calculations as well as observationally-constrained simulations of Pleistocene and Holocene dust deposition suggest that soil erodibility is extremely heterogenous (Zender et al., 2003b; Mahowald et al., 2006b), so any conclusions drawn from this result must be considered tenuous.

The consequence of doubling or halving peat carbon accumulation rates is to double or halve dust deposition rate respectively. Doubling dust deposition produces maximum rates in excess of 40 g $m^{-2}yr^{-1}$. Currently, values of this magnitude (Mahowald et al., 2006b) only occur in areas too arid to support peat formation (Yu et al., 2010). It therefore seems unlikely that peat carbon accumulation rates were significantly higher than those observed in the Holocene. Halving dust deposition rate produces values that still fall within the global range

of values encountered in temperate climates and at high latitude today (Mahowald et al., 2006b). However, whether the values are halved or doubled, the conclusion that ash concentrations in Permian coal display global patterns consistent, in magnitude and scale, with a mineral dust origin remains unchanged.

Different dust deposition rates would only be expected if the physical process of dust generation, atmospheric entrainment and transport were very different in the Permian. Wind speed which exercises a strong control on dust entrainment and transport (Mahowald et al., 2014) is predicted to have been in a range similar to present day values during the Permian (Gibbs et al., 2002) and the similarity between estimated Permian and modern dust deposition rates supports this prediction. A possible confounding factor is whether or not the peatland productivity is linked to the dust supply. If this were the case then mineral dust deposition rates may have been underestimated in areas of high dust deposition rate and vice versa. If present it is unlikely that this effect would be substantial as it has not been observed in peatland today.

In one instance, the coal derived data also can be compared with DAR estimates from other techniques. From Late Carboniferous/Early Permian coals from 5° N 80° W in equatorial Pangea, dust accumulation rates of 16–25 g m^{-2} yr^{-1} are inferred. This is fully consistent with the high dust deposition rates estimated for an offshore atoll in western equatorial Pangaea during Early Permian glacial intervals (Sur et al., 2010). Early Permian dust deposition rates in the interior of western equatorial Pangaea can be estimated from loess–palaeosol couplets in the Maroon Formation (Soreghan et al., 2014). If it is assumed that these couplets represent obliquity cycles of 43 kyr, their characteristic thickness is 2 m, and their density is 2000 kg m^{-3}, the inferred dust deposition rate averages 93 g m^{-2} yr^{-1}, a high deposition rate that would be expected for a dust sink in the arid continental interior.

That the dust deposition rate in coals to the east of this area is closer to that in offshore areas may imply greater distance from the dust source region.

4. Implications and Conclusions

A remarkable aspect of the observations is the presence of a pattern in coal data that spans a considerable period (Fig. 2); 47 Myr for the entire Permian dataset and 27 Myr for the Gondwana coal data. This would not be expected if concentrations of atmospheric dust and source regions displayed high spatial and temporal variability. The presence of this pattern implies the existence of prolonged stable dust plumes during periods of Permian peat deposition. The stability of these dust plumes also implies significant and sustained windborne dust and phytonutrient load to the Palaeo-Tethys that could have contributed to eutrophication and development of anoxia in this enclosed marine basin, a process considered by some to have contributed to the end-Permian mass-extinction (Knoll et al., 2007).

Another important conclusion is that the global processes of dust deposition can reasonably account for the large scale differences in coal ash concentration during the Permian. Inevitably this leads to the consideration of what might be achieved at higher resolution with a more refined stratigraphy within single coal seams or successive seams. In combination with a reasoned estimate of the time, which in the case of a 1.5m thick, mid-latitude, bituminous coal could represent more than 100 kyr, it should be possible to resolve variable DAR over the duration of the coal seam(s) and associated climate cycles. Furthermore coal could, in principle, also yield geochemical data on dust provenance.

From an economic perspective, the dominant dust control upon coal quality is likely to have consequences for hydrocarbon and coal exploration. In the case of Permian coal, a combination of global palaeoclimatic and palaeogeographic factors would appear to render large areas incapable of producing high quality coal. With further high resolution study

within developed coal basins, lower dust intervals may be identified and targeted for future exploration and mine expansion. In the case of economically important oceanic anoxic events, a better knowledge of the amount, timing and distribution of aeolian derived nutrient load to restricted basins may also be of use in identifying and understanding the distribution of hydrocarbon source rocks.

In summary these results demonstrate the capacity to use coal deposits to constrain patterns and quantify rates of dust deposition. This opens the door to using coal to explore, at higher resolution, the climatic and environmental effect of changes in Permian dust load, including the role of dust in the Permian deglaciation. More significant is the potential to use coal derived dust records in conjunction with other climate proxies and models to extend our understanding of the role of atmospheric dust in biogeochemical cycles and palaeoclimate from the Quaternary to the Carboniferous.

Acknowledgements: This work was jointly funded by the Faculty of Engineering University of Nottingham, the Nottingham Centre for Carbon Capture and Storage, and the U.S. National Science Foundation (EAR-0745961, EAR-0932946, EAR-1003509, and EAR-1337363) High-performance computing support was provided by NCAR's Computational and Information Systems Laboratory, sponsored by the National Science Foundation. PaleoGIS was supplied free under an academic license.

Figure Captions:

Fig. 1 – Plot of titanium concentration vs. ash concentration showing regression lines and statistical summary for different regions within the dataset. Data from South China displays

evidence of a markedly different trend interpreted as being indicative of the reported influence of titanium enriched volcanic ash on this coal (Dai et al., 2012). Data from Brazil occurs in two clusters, one that aligns with the global trend and another that may indicate the influence of a titanium depleted source. (2 Column Colour)

Fig. 2 – Stratigraphic context of the Permian coal samples used in this study *after Langford et al., 1992.* Gradational fading of the shaded bars represents decreasing seam thickness and abundance. C = Carboniferous, Trias = Triassic, Gz = Gzhelian, Wuchia = Wuchiapingian, Ch = Changhsingian, Ind = Induan (2 Column Colour)

Fig. 3 - Map of the standard error in the ash concentration prediction surface contour maps (Fig. 1). The same pattern of uncertainty applies to the derived map of dust (Fig. 4B). (2 Column Greyscale)

Fig. 4 - Contoured prediction surface maps of A) ash concentration and B) calculated dust accumulation rate. Maps are plotted on the mid-Permian Kungurian continental configuration. (2 Column Colour)

Fig. 5 - Simulated dust emission rates under A) greenhouse.noglaciation and B) icehouse.glaciation.polar conditions. Maps are plotted on the mid-Permian Sakmarian-Artinskian continental configuration. Arid marks correspond to mean annual precipitation < 400 mm. This is the boundary between sub-arid and sub-humid conditions chosen by Rea (1994). (2 Column Colour)

Fig. 6 - Simulated DAR under A) greenhouse.noglaciation and B) icehouse.glaciation.polar conditions. Maps are plotted on the mid-Permian Sakmarian-Artinskian continental configuration. Arid marks correspond to mean annual precipitation < 400 mm. This is the

boundary between sub-arid and sub-humid conditions chosen by Rea (1994). (2 Column Colour)

Supplementary Table 1 –Collated ash data on global Permian coal deposits.

Supplementary Table 2 – Collated titanium data on global Permian coal deposits

Supplementary References – References to the source of all data in Table 1.

References

Beerling, D.J., Woodward, F.I., 2001. Vegetation and the terrestrial carbon cycle; Modelling the first 400 million years. Cambridge University Press, Cambridge.

Blakey, R. 'Global Palaeogeographic Views Of Earth History-Late Precambrian To Recent'. *Cpgeosystems.com*. N.p., 2015. Web. 15 June 2015.

Boucot, A.J., Xu, C., Scotese, C.R., 2013. Phanerozoic paleoclimate: an atlas of lithologic indicators of climate. SEPM Concepts in Sedimentology and Paleontology 11.

Boyd, P.W., Ellwood, M.J., 2010. The biogeochemical cycle of iron in the ocean. Nature Geoscience 3, 675-682, Doi 10.1038/Ngeo964.

Bragg, L., Oman, J., Tewalt, S., Oman, C., Rega, N., Washington, P., Finkelman, R., 1998. U.S. Geological Survey Coal Quality (COALQUAL) Database: Version 2.0, Open File Report U.S.Geological Survey.

Bristow, C.S., Hudson-Edwards, K.A., Chappell, A., 2010. Fertilizing the Amazon and equatorial Atlantic with West African dust. Geophysical Research Letters 37, Doi 10.1029/2010gl043486.

Clymo, R.S., Turunen, J., Tolonen, K., 1998. Carbon accumulation in peatland. Oikos 81, 368-388.

Dai, S.F., Ren, D.Y., Chou, C.L., Finkelman, R.B., Seredin, V.V., Zhou, Y.P., 2012. Geochemistry of trace elements in Chinese coals: A review of abundances, genetic types, impacts on human health, and industrial utilization. International Journal of Coal Geology 94, 3-21.

Einsele, G., 2000. Sedimentary Basins: evolution, facies, and sediment budget. Springer-Verlag, Berlin.

Evan, A.T., Foltz, G.R., Zhang, D.X., Vimont, D.J., 2011. Influence of African dust on ocean-atmosphere variability in the tropical Atlantic. Nature Geoscience 4, 762-765, Doi 10.1038/Ngeo1276.

Gabbott, S.E., Zalasiewicz, J., Aldridge, R.J., Theron, J.N., 2010. Eolian input into the Late Ordovician postglacial Soom Shale, South Africa. Geology 38, 1103-1106.

Gibbs, M.T., Rees, P.M., Kutzbach, J.E., Ziegler, A.M., Behling, P.J., Rowley, D.B., 2002. Simulations of Permian climate and comparisons with climate-sensitive sediments. Journal of Geology 110, 33-55.

Ginoux, P., Chin, M., Tegen, I., Prospero, J.M., Holben, B., Dubovik, O., Lin, S.J., 2001. Sources and distributions of dust aerosols simulated with the GOCART model. Journal of Geophysical Research-Atmospheres 106, 20255-20273.

Glasspool, I.J., 2003. Hypautochthonous-allochthonous coal deposition in the Permian, South African, Witbank Basin No. 2 seam; a combined approach using sedimentology, coal petrology and palaeontology. International Journal of Coal Geology 53, 81-135.

Heavens, N.G., Mahowald, N.M., Soreghan, G.S., Soreghan, M.J., Shields, C.A., 2015. A model-based evaluation of tropical climate in Pangaea during the late Palaeozoic icehouse. Paleogeography Paleoclimatology Paleoecology 425, 109-127.

Jha, N., Sabina, K.P., Aggarwal, N., Mahesh, S., 2014. Late Permian Palynology and depositional environment of Chintalapudi sub basin, Pranhita-Godavari basin, Andhra Pradesh, India. Journal of Asian Earth Science 79, 382-399.

Kaplan, J.O., Bigelow, N.H., Prentice, I.C., Harrison, S.P., Bartlein, P.J., Christensen, T.R., Cramer, W., Matveyeva, N.V., McGuire, A.D., Murray, D.F., Razzhivin, V.Y., Smith, B., Walker, D.A., Anderson, P.M., Andreev, A.A., Brubaker, L.B., Edwards, M.E., Lozhkin, A.V., 2003. Climate change and Arctic ecosystems: 2. Modeling, paleodata-model comparisons, and future projections. Journal of Geophysical Research-Atmospheres 108, Doi 10.1029/2002jd002559.

Knoll, A.H., Barnbach, R.K., Payne, J.L., Pruss, S., Fischer, W.W., 2007. Paleophysiology and end-Permian mass extinction. Earth Planetary Science Letters 256, 295-313.

Kok, J.F., 2011. A scaling theory for the size distribution of emitted dust aerosols suggests climate models underestimate the size of the global dust cycle. Proceedings of the National Academy of Sciences of the United States of America 108, 1016-1021.

Lambert, F., Delmonte, B., Petit, J.R., Bigler, M., Kaufmann, P.R., Hutterli, M.A., Stocker, T.F., Ruth, U., Steffensen, J.P., Maggi, V., 2008. Dust-climate couplings over the past 800,000 years from the EPICA Dome C ice core. Nature 452, 616-619.

Langford, R.P., Cairncross, B., Friedrich, M., 1992. Permian Coal and Palaeogeography of Gondwana. Bureau of Mineral Resources, Geology and Geophysics, Canberra.

Large, D.J., Marshall, C., 2014. Use of carbon accumulation rates to estimate the duration of coal seams and the influence of atmospheric dust deposition on coal composition. Geological Society, London, Special Publications 10.1144/sp404.15, 10.1144/sp404.15.

Lawrence, C.R., Neff, J.C., 2009. The contemporary physical and chemical flux of aeolian dust: A synthesis of direct measurements of dust deposition. Chemical Geology 267, 46-63, 10.1016/j.chemgeo.2009.02.005.

Le Roux, G., Fagel, N., De Vleeschouwer, F., Krachler, M., Debaille, V., Stille, P., Mattielli, N., van der Knaap, W.O., van Leeuwen, J.F.N., Shotyk, W., 2012. Volcano- and climate-driven changes in atmospheric dust sources and fluxes since the Late Glacial in Central Europe. Geology 40, 335-338.

Li, Y.-H., 2000. A compendium of geochemistry, from solar nebula to the human brain. Princeton University Press.

Luo, C., Mahowald, N.M., del Corral, J., 2003. Sensitivity study of meteorological parameters on mineral aerosol mobilization, transport, and distribution. Journal of Geophysical Research-Atmospheres 108, Doi 10.1029/2003jd003483.

Maher, B.A., Prospero, J.M., Mackie, D., Gaiero, D., Hesse, P.P., Balkanski, Y., 2010. Global connections between aeolian dust, climate, and ocean biogeochemistry at the present day and the last glacial maximum. Earth Science Reviews 99, 61–97.

Mahowald, N., Albani, S., Kok, J.F., Engelstaeder, S., Scanza, R., Ward, D.S., Flanner, M.G., 2014. The size distribution of desert dust aerosols and its impact on the Earth system. Aeolian Research 15, 53-71, DOI 10.1016/j.aeolia.2013.09.002.

Mahowald, N.M., Lamarque, J.F., Tie, X.X., Wolff, E., 2006a. Sea-salt aerosol response to climate change: Last Glacial Maximum, preindustrial, and doubled carbon dioxide climates. Journal of Geophysical Research-Atmospheres 111, Doi 10.1029/2005jd006459.

Mahowald, N.M., Muhs, D.R., Levis, S., Rasch, P.J., Yoshioka, M., Zender, C.S., Luo, C., 2006b. Change in atmospheric mineral aerosols in response to climate: Last glacial period, preindustrial, modern, and doubled carbon dioxide climates. Journal of Geophysical Research-Atmospheres 111, Doi 10.1029/2005jd006653.

McGee, D., deMenocal, P.B., Winckler, G., Stuut, J.B.W., Bradtmiller, L.I., 2013. The magnitude, timing and abruptness of changes in North African dust deposition over the last 20,000 yr. Earth Planetary Science Letters 371, 163-176.

Okin, G.S., 2008. A new model of wind erosion in the presence of vegetation. Journal of Geophysical Research-Earth 113, Doi 10.1029/2007jf000758.

Okin, G.S., Baker, A.R., Tegen, I., Mahowald, N.M., Dentener, F.J., Duce, R.A., Galloway, J.N., Hunter, K., Kanakidou, M., Kubilay, N., Prospero, J.M., Sarin, M., Surapipith, V., Uematsu, M., Zhu, T., 2011. Impacts of atmospheric nutrient deposition on marine productivity: Roles of nitrogen, phosphorus, and iron. Global Biogeochemical Cycles 25, Doi 10.1029/2010gb003858.

Patterson, E., 2011. Fluctuating dust in the late Paleozoic ice house: records from an oceanic atoll, Akiyoshi, Japan. University of Oklahoma, p. 115.

Prenni, A.J., Petters, M.D., Kreidenweis, S.M., Heald, C.L., Martin, S.T., Artaxo, P., Garland, R.M., Wollny, A.G., Poschl, U., 2009. Relative roles of biogenic emissions and Saharan dust as ice nuclei in the Amazon basin. Nature Geoscience 2, 401-404, Doi 10.1038/Ngeo517.

Retallack, G.J., 1999. Permafrost palaeoclimate of Permian palaeosols in the Gerringong volcanic facies of New South Wales. Australian Journal of Earth Science 46, 11-22.

Retallack, G.J., 2011. Neoproterozoic loess and limits to snowball Earth. Journal of the Geological Society 168, 289-307.

Retallack, G.J., 2012. Were Ediacaran siliciclastics of South Australia coastal or deep marine? Sedimentology 59, 1208-1236.

Retallack, G.J., Smith, R.M.H., Ward, P.D., 2003. Vertebrate extinction across Permian-Triassic boundary in Karoo Basin, South Africa. Geological Society of America Bulletin 115, 1133-1152.

Scotese, C.R., 2001. Atlas of Earth History, Volume 1, Paleogeography, Palaeomap Project, Arlington, Texas.

Silva, M.B., Kalkreuth, W., 2005. Petrological and geochemical characterization of Candiota coal seams, Brazil - Implication for coal facies interpretations and coal rank. International Journal of Coal Geology 64, 217-238.

Soreghan, G.S., Soreghan, M.J., Hamilton, M.A., 2008a. Origin and significance of loess in late Paleozoic western Pangaea: A record of tropical cold? Paleogeography Paleoclimatology Paleoecology 268, 234-259.

Soreghan, G.S., Soreghan, M.J., Poulsen, C.J., Young, R.A., Eble, C.F., Sweet, D.E., Davogustto, O.C., 2008b. Anomalous cold in the Pangaean tropics. Geology 36, 659-662.

Soreghan, G.S., Sweet, D.E., Heavens, N.G., 2014. Upland Glaciation in Tropical Pangaea: Geologic Evidence and Implications for Late Paleozoic Climate Modeling. Journal of Geology 122, 137-163.

Stagner, A.F., 2008. Eolian silt in upper Paleozoic carbonates of the Bird Spring Formation (Arrow Canyon, Nevada): implications for climate-controlled sedimentation. University of Oklahoma, p. 115.

Sugden, D.E., McCulloch, R.D., Bory, A.J.M., Hein, A.S., 2009. Influence of Patagonian glaciers on Antarctic dust deposition during the last glacial period. Nature Geoscience 2, 281-285, Doi 10.1038/Ngeo474.

Sur, S., Soreghan, M.J., Soreghan, G.S., Stagner, A.F., 2010. Extracting the Silicate Mineral Fraction from Ancient Carbonate: Assessing the Geologic Record of Dust. Journal of Sedimentary Research 80, 763-769.

Tewalt, S.J., Belkin, H.E., san Filipo, J.R., Merrill, M.D., Palmer, C.A., Warwick, P.D., Karlsen, A.W., Finkelman, R.B., Park, A.J., 2010. Chemical analyses in the World Coal Quality Inventory, version 1, U S Geological Survey Open File Report, p. 4.

Thomas, L., 2013. Coal Geology. John Wiley & Sons, Chichester, West Sussex.

Vassilev, S.V., Tascon, J.M.D., 2003. Methods for characterization of inorganic and mineral matter in coal: A critical overview. Energy and Fuels 17, 271-281.

Ward, C.R., 2002. Analysis and significance of mineral matter in coal seams. International Journal of Coal Geology 50, 135-168.

Yang, J.H., Cawood, P.A., Du, Y.S., Feng, B., Yan, J.X., 2014. Global continental weathering trends across the Early Permian glacial to postglacial transition: Correlating high- and low-paleolatitude sedimentary records. Geology 42, 835-838, Doi 10.1130/G35892.1.

Yoshioka, M., Mahowald, N.M., Conley, A.J., Collins, W.D., Fillmore, D.W., Zender, C.S., Coleman, D.B., 2007. Impact of desert dust radiative forcing on Sahel precipitation: Relative importance of dust compared to sea surface temperature variations, vegetation changes, and greenhouse gas warming. Journal of Climatology 20, 1445-1467.

Yu, Z.C., Loisel, J., Brosseau, D.P., Beilman, D.W., Hunt, S.J., 2010. Global peatland dynamics since the Last Glacial Maximum. Geophysical Research Letters 37, Doi 10.1029/2010gl043584.

Zaccone, C., Pabst, S., Senesi, G.S., Shotyk, W., Miano, T.M., 2013. Comparative evaluation of the mineralogical composition of Sphagnum peat and their corresponding humic acids, and implications for understanding past dust depositions. Quaternary International 306, 80-87, DOI 10.1016/j.quaint.2013.04.017.

Zender, C.S., Bian, H.S., Newman, D., 2003a. Mineral Dust Entrainment and Deposition (DEAD) model: Description and 1990s dust climatology. Journal of Geophysical Research-Atmospheres 108, Doi 10.1029/2002jd002775.

Zender, C.S., Newman, D., Torres, O., 2003b. Spatial heterogeneity in aeolian erodibility: Uniform, topographic, geomorphic, and hydrologic hypotheses. Journal of Geophysical Research-Atmospheres 108.

CV

Chris Marshall graduated with a BSc in Environmental Geology and an MSc in Geochemistry from the University of Leeds in 2009, followed by a PhD from the University of Nottingham on the geochemistry and petrology of coal from Central Tertiary Basin on Svalbard in 2013. His current research interests include unconventional source rock potential and maturity, the sedimentological and stratigraphic interpretation of coal bearing basins and coal as a record of past environmental change.

David Large graduated with a BSc in Applied Geology from the University of Strathclyde in 1987, followed by a PhD from the University of Cambridge in 1992 on metamorphic petrology. Since then he has applied his interest in geochemistry and petrology to a range of topics including black shale copper deposits, Holocene peat and utilising coal to understand Earth systems.

Nicholas Heavens is Research Assistant Professor of Planetary Science at Hampton University. He holds a Ph.D. in planetary science from the California Institute of Technology (2010). His research focuses on the present day weather of Mars but keeps expanding to other dusty times and places.

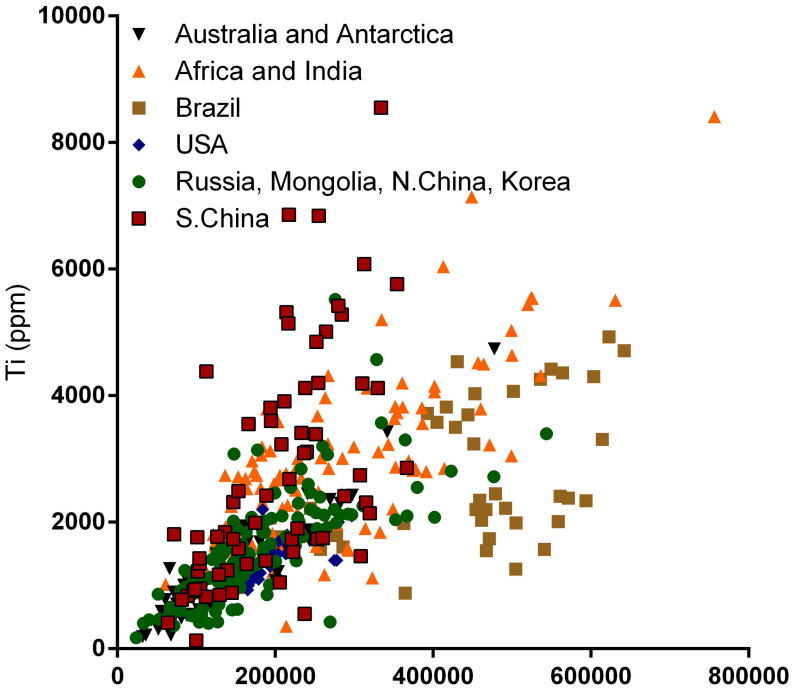

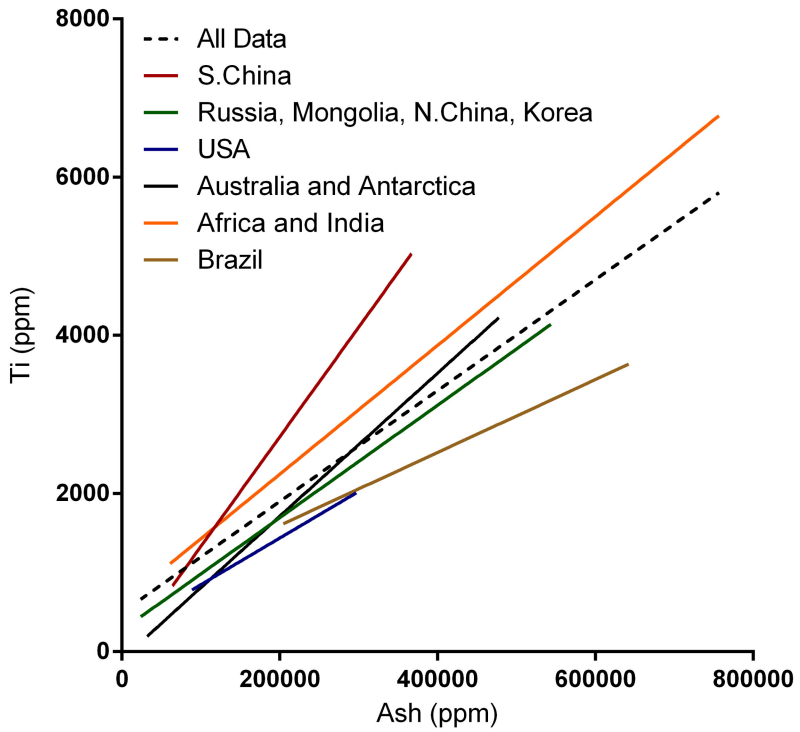

Location	Y- Intercept	Slope	r^2	P-Value
All Data	496.2	0.007	0.45	<0.0001
Brazil	675.9	0.004	0.21	0.0037
Africa and India	615.4	0.008	0.61	<0.0001
Australia and Antarctica	-93.61	0.009	0.86	<0.0001
USA	258.3	0.005	0.53	<0.0001
Russia, Mongolia, N.China, Korea	272.1	0.007	0.55	<0.0001
South China	-55.76	0.014	0.36	<0.0001

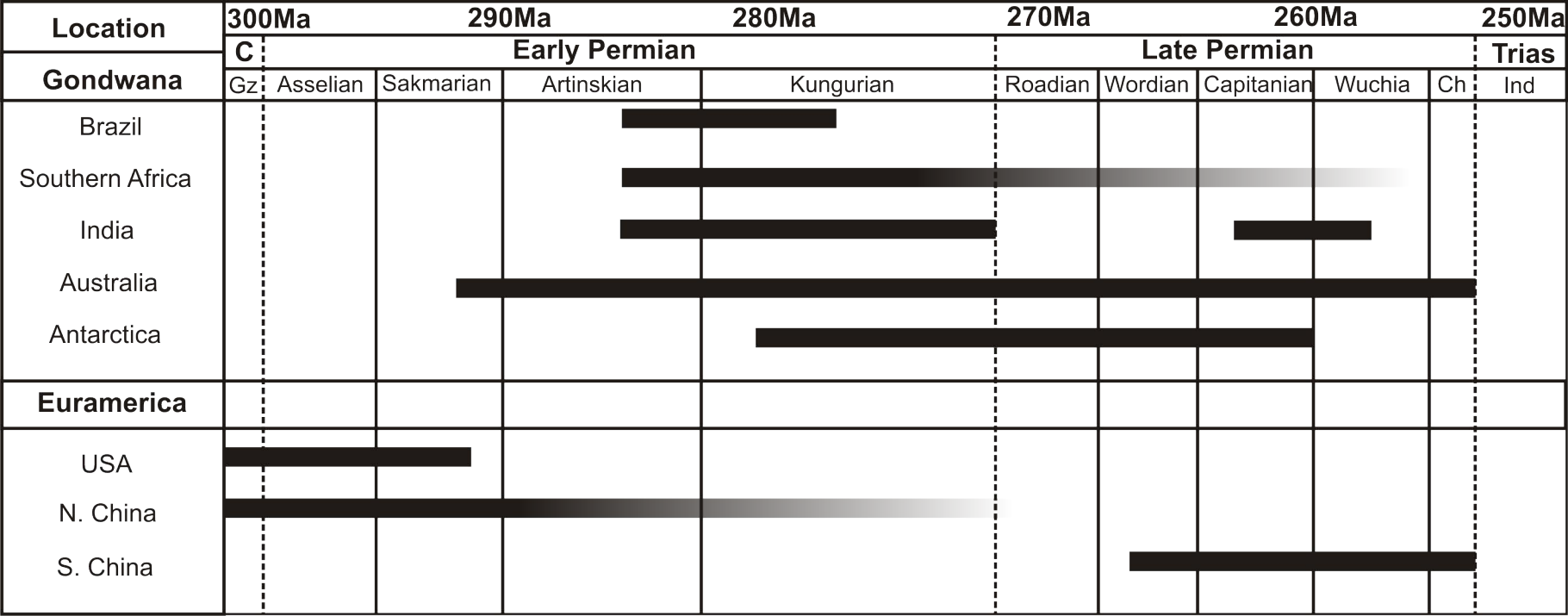
Location
300Ma
290Ma
280Ma
270Ma
260Ma
250Ma
C
Early Permian
Late Permian
Trias
Gondwana
Gz
Asselian
Sakmarian
Artinskian
Kungurian
Roadian
Wordian
Capitanian
Wuchia
Ch
Ind
Brazil
Southern Africa
India
Australia
Antarctica
Euramerica
USA
N. China
S. China

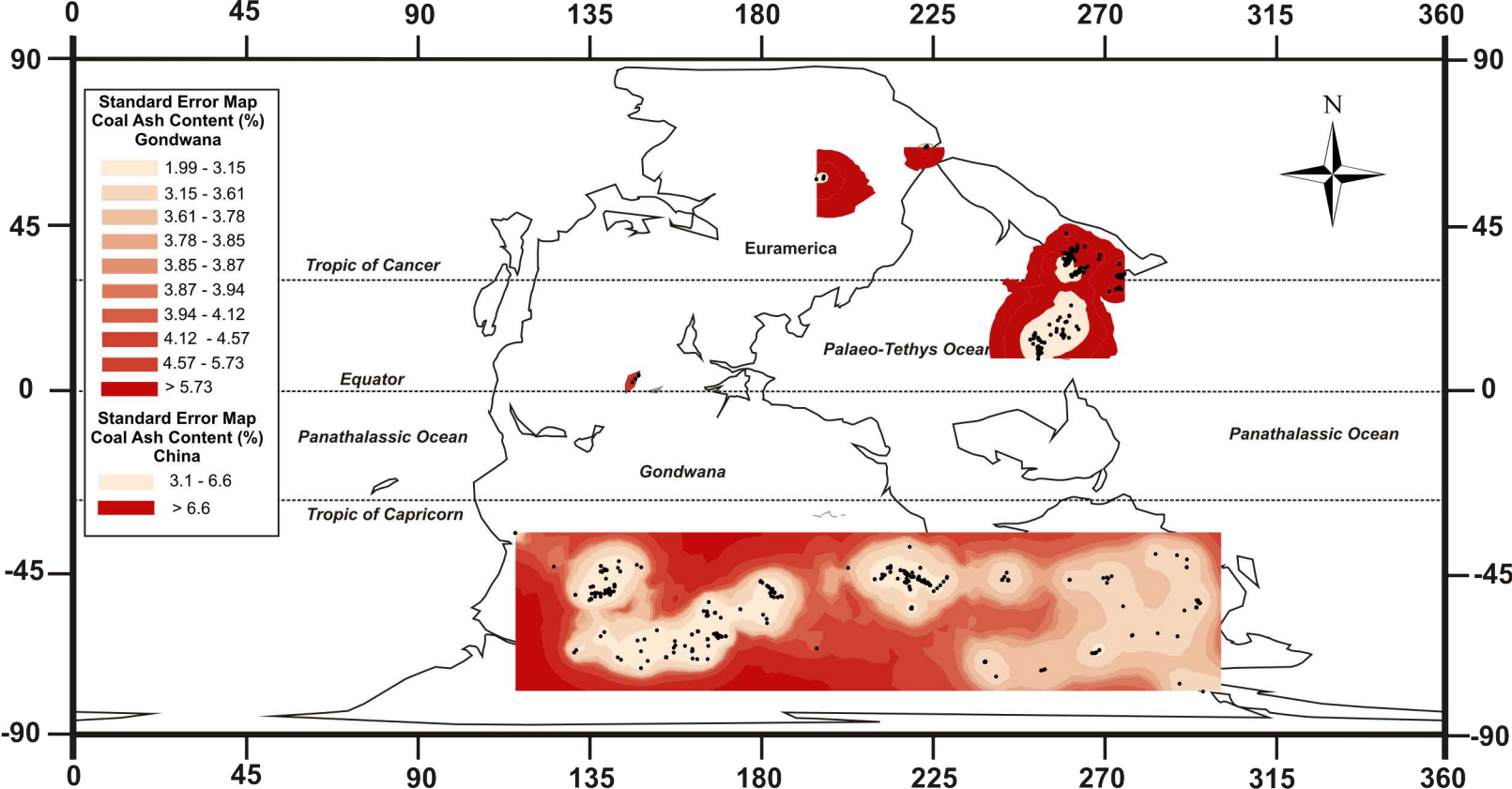
Standard Error Map
Coal Ash Content (%)
Gondwana
1.99 - 3.15
3.15 - 3.61
3.61 - 3.78
3.78 - 3.85
3.85 - 3.87
3.87 - 3.94
3.94 - 4.12
4.12 - 4.57
4.57 - 5.73
> 5.73
Standard Error Map
Coal Ash Content (%)
China
3.1 - 6.6
> 6.6
N
Euramerica
Tropic of Cancer
Palaeo-Tethys Ocean
Equator
Panathalassic Ocean
Gondwana
Panathalassic Ocean
Tropic of Capricorn
0
45
90
135
180
225
270
315
360
90
45
0
-45
-90

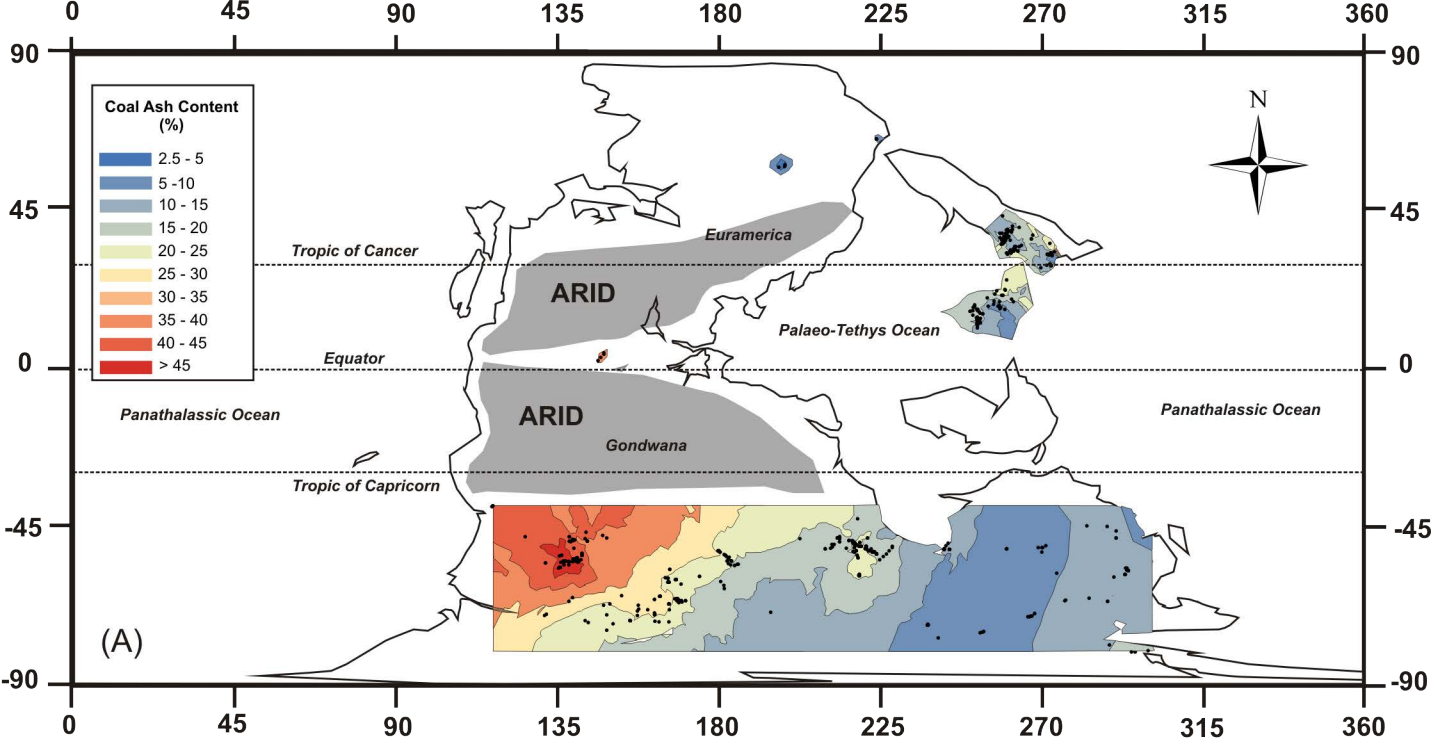
Coal Ash Content (%)
2.5 - 5
5 -10
10 - 15
15 - 20
20 - 25
25 - 30
30 - 35
35 - 40
40 - 45
> 45
N
Euramerica
ARID
Palaeo-Tethys Ocean
Tropic of Cancer
Equator
Panathalassic Ocean
ARID
Gondwana
Panathalassic Ocean
Tropic of Capricorn
(A)
0
45
90
135
180
225
270
315
360
90
45
0
-45
-90

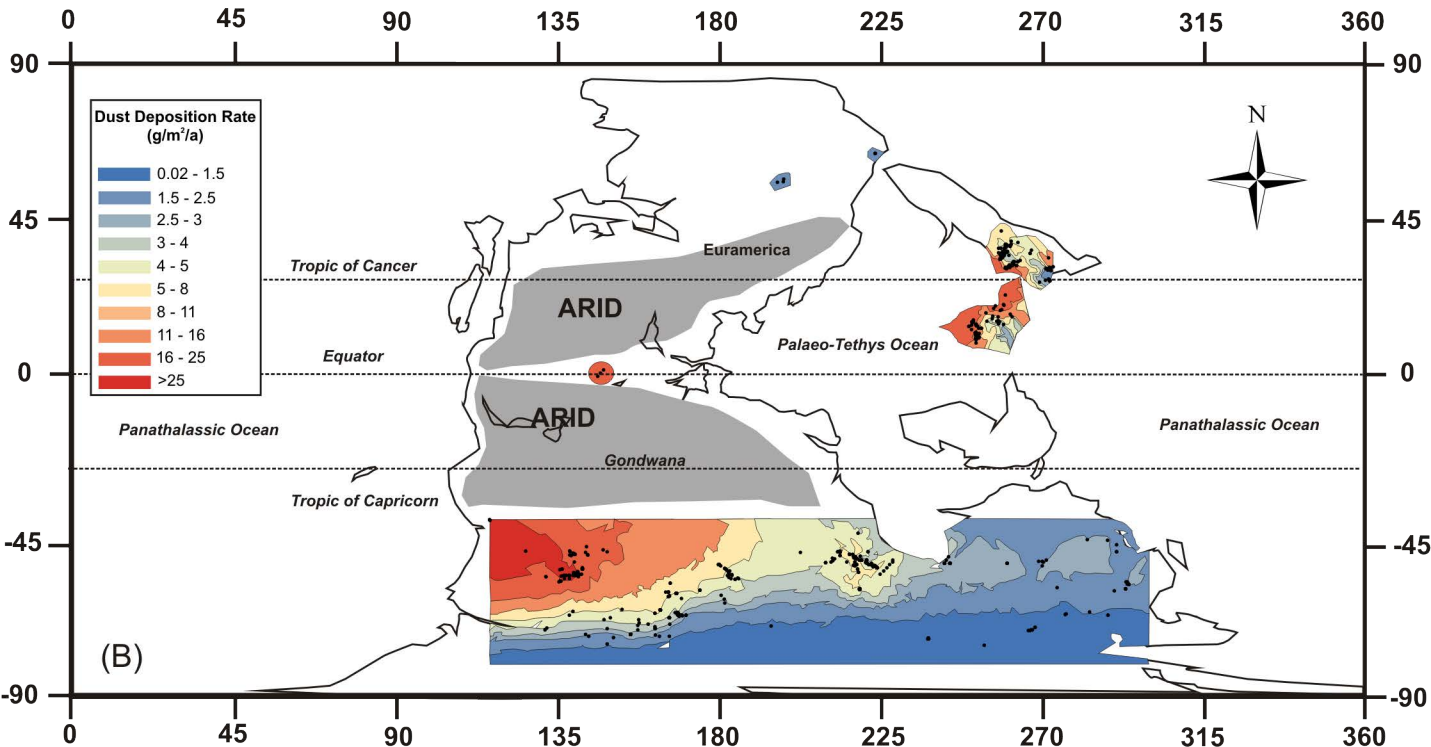
Dust Deposition Rate (g/m²/a)
0.02 - 1.5
1.5 - 2.5
2.5 - 3
3 - 4
4 - 5
5 - 8
8 - 11
11 - 16
16 - 25
>25
N
Euramerica
ARID
Palaeo-Tethys Ocean
Tropic of Cancer
Equator
Panathalassic Ocean
ARID
Gondwana
Panathalassic Ocean
Tropic of Capricorn
(B)
0
45
90
135
180
225
270
315
360
90
45
0
-45
-90

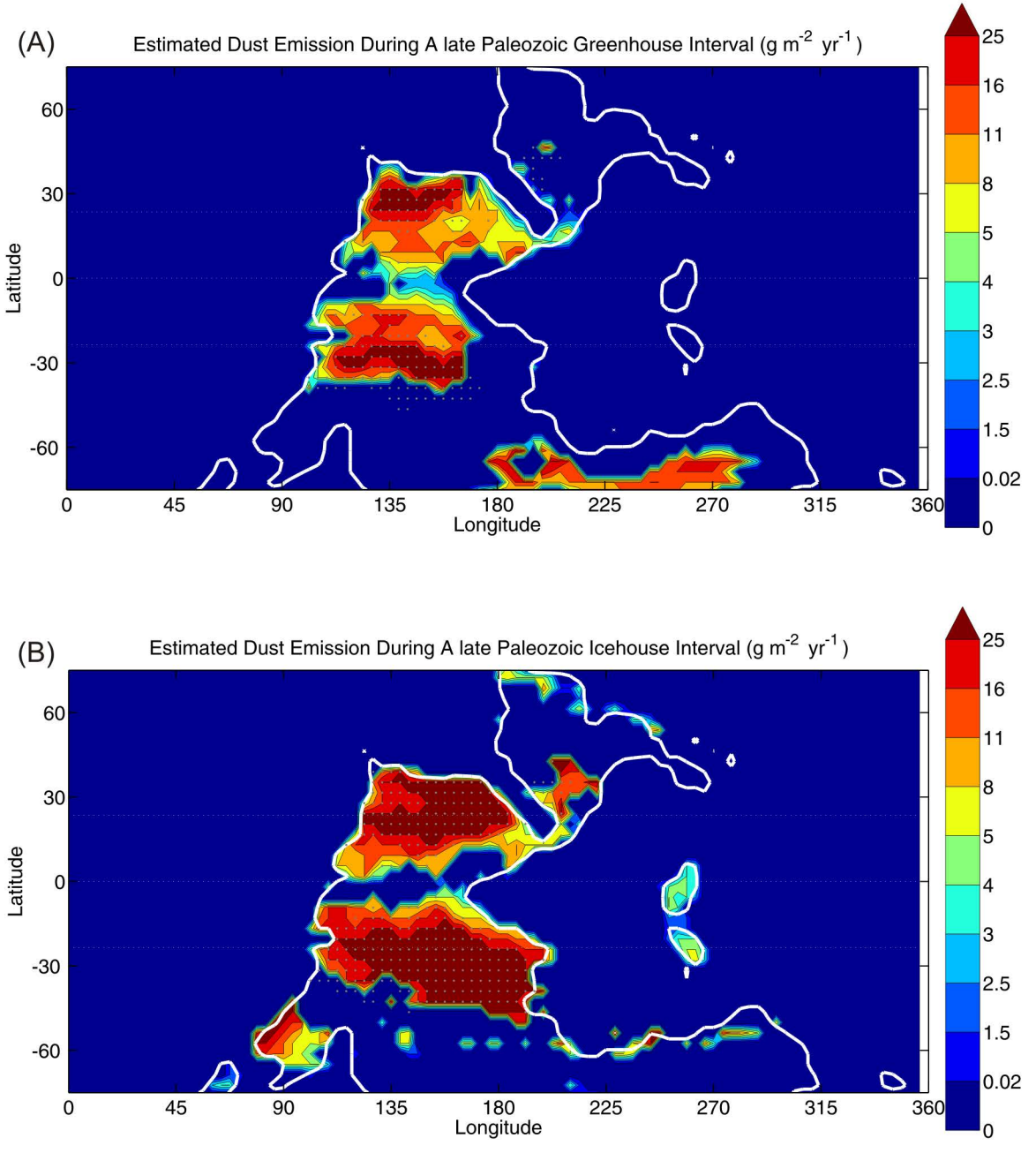
(A)
Estimated Dust Emission During A late Paleozoic Greenhouse Interval (g m-2 yr-1)
Latitude
Longitude
60
30
0
-30
-60
0
45
90
135
180
225
270
315
360
25
16
11
8
5
4
3
2.5
1.5
0.02
0
(B)
Estimated Dust Emission During A late Paleozoic Icehouse Interval (g m-2 yr-1)
Latitude
Longitude
60
30
0
-30
-60
0
45
90
135
180
225
270
315
360
25
16
11
8
5
4
3
2.5
1.5
0.02
0

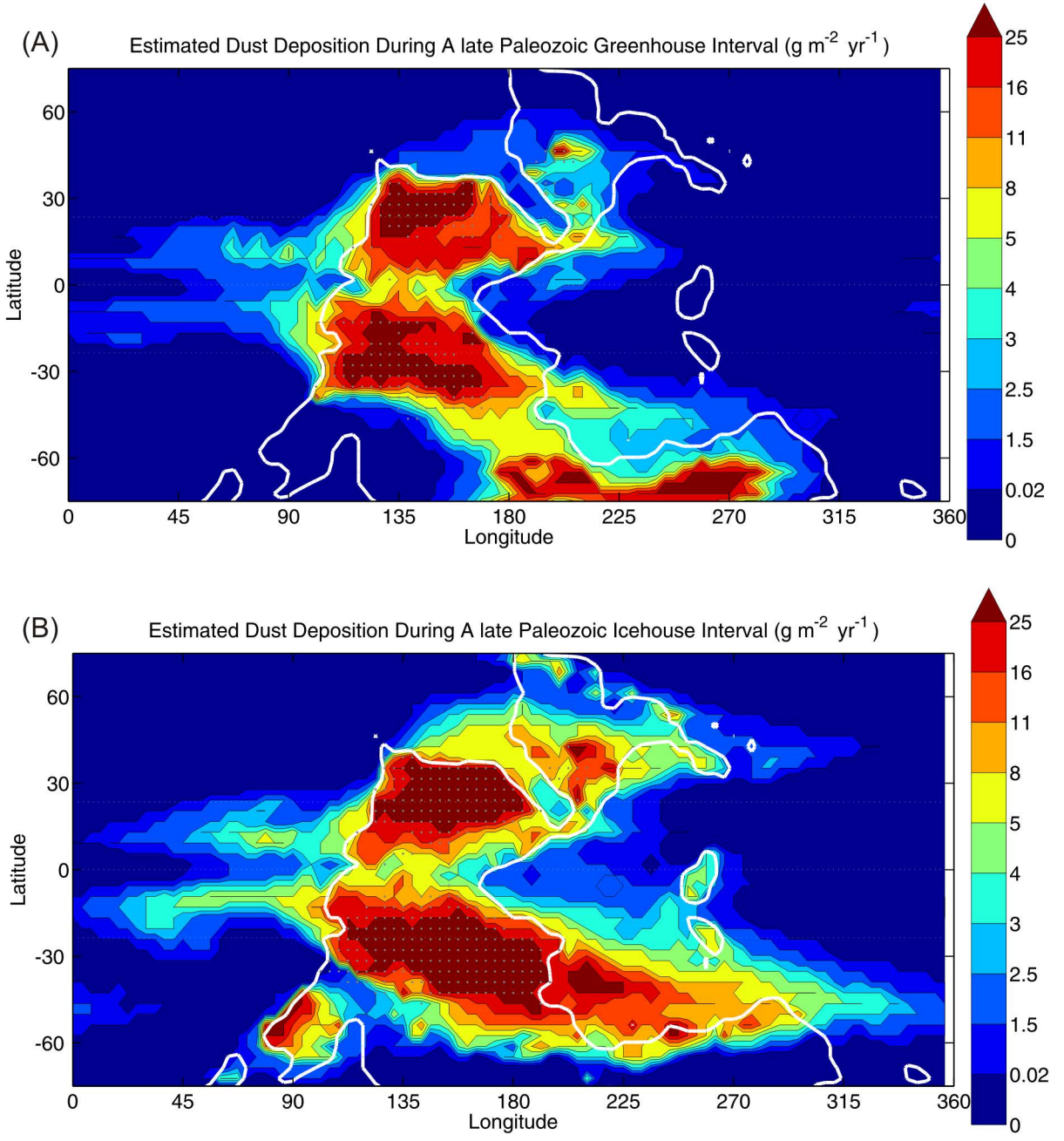
(A)
Estimated Dust Deposition During A late Paleozoic Greenhouse Interval (g m-2 yr-1)
Latitude
60
30
0
-30
-60
0
45
90
135
180
225
270
315
360
Longitude
25
16
11
8
5
4
3
2.5
1.5
0.02
0
(B)
Estimated Dust Deposition During A late Paleozoic Icehouse Interval (g m-2 yr-1)
Latitude
60
30
0
-30
-60
0
45
90
135
180
225
270
315
360
Longitude
25
16
11
8
5
4
3
2.5
1.5
0.02
0